THE ASTROPHYSICAL JOURNAL, 548:787–799, 2001 February 20

ON THE SYNCHROTRON SELF-COMPTON EMISSION FROM RELATIVISTIC SHOCKS AND ITS IMPLICATIONS FOR GAMMA-RAY BURST AFTERGLOWS

RE'EM SARI AND ANN A. ESIN[1]
130-33 California Institute of Technology, Pasadena, CA 91125; sari@tapir.caltech.edu, aidle@tapir.caltech.edu
Received 2000 May 15; accepted 2000 August 23

ABSTRACT

We consider the effects of inverse Compton scattering of synchrotron photons from relativistic electrons in γ-ray burst (GRB) afterglows. We compute the spectrum of the inverse Compton emission and find that it can dominate the total cooling rate of the afterglow for several months or even years after the initial explosion. We demonstrate that the presence of strong inverse Compton cooling can be deduced from the effect it has on the time evolution of the cooling break in the synchrotron spectral component, and therefore on the optical and X-ray afterglow light curves. We then show how the physical interpretation of the observed characteristics of the synchrotron spectrum must be modified to take into consideration this extra source of cooling and give a revised prescription for computing physical parameters characterizing the expanding shock wave from the observed quantities. We find that for a given set of observables (synchrotron break frequencies and fluxes) there is either no consistent physical interpretation or two of them. Finally we discuss the prospects of directly detecting the inverse Compton emission with *Chandra*. We argue that such a detection is possible for GRBs exploding in a reasonably dense ($n \gtrsim 1$ cm^{-3}) medium.

Subject headings: gamma rays: bursts — radiation mechanisms: nonthermal

1. INTRODUCTION

It is widely accepted that the emission from γ-ray burst (GRB) afterglows is produced in relativistic shocks, as the ejecta from an underlying explosion expands into the surrounding medium (e.g., Piran 1999, and references therein), as predicted by Paczyński & Rhoads (1993), Katz (1994), Mészáros & Rees (1997), and Vietri (1997). In the standard picture, the ambient electrons are accelerated in the shock front to highly relativistic energies, with their Lorentz factors described by a power-law distribution above some minimum value. Besides particle acceleration, the shock is also responsible for the creation of reasonably strong magnetic fields. Under these conditions synchrotron radiation, whose spectrum and light curves were described by Sari, Piran, & Narayan (1998), is produced.

Though GRBs and their afterglows are optically thin to electron scattering for years after the initial explosion, some synchrotron photons will Compton scatter on the shock-accelerated electrons, producing an additional inverse Compton component at higher energies (Panaitescu & Mészáros 1998; Wei & Lu 1998; Totani 1998; Chiang & Dermer 1999; Dermer, Chiang, & Mitman 2000b; Dermer, Bottcher, & Chiang 2000a; Panaitescu & Kumar 2000; similar calculations in other astrophysical contexts were done by Blandford & McKee 1977 for both a constant density and a windlike ambient medium). Since only a negligible fraction of the synchrotron photons will be scattered, this will have no direct effect on the shape of the synchrotron spectrum. However, the ratio of inverse Compton to synchrotron luminosities is equal to the square root of the ratio of the electron and magnetic energy densities behind the shock front (Sari, Narayan, & Piran 1996). Since this number can be significantly above unity, this implies that the electron cooling rate via inverse Compton scattering of synchrotron photons must be considered in order to create a realistic physical description of the GRB afterglow emission.

In their paper, Panaitescu & Kumar (2000) give a detailed treatment of the inverse Compton emission from GRB afterglows. Here we extend their analysis, concentrating on the implications of this cooling process for the observable properties of these objects. We start by calculating the spectrum of the inverse Compton emission in § 2. The gross power-law features of this spectral component are the same as those in Panaitescu & Kumar (2000). However, here we show that the broken power law is not an adequate approximation above the peak frequency, where the presence of the logarithmic terms may introduce large corrections to the predicted flux levels. These extra terms also serve to smooth out the resulting spectrum and high-energy light curves, eliminating sharp power-law breaks in the theoretical predictions.

In § 3 we discuss in detail the effects of inverse Compton cooling on the afterglow evolution. We show that, instead of the two standard stages of evolution, corresponding to fast and slow cooling, we now have three stages. This occurs because the slow-cooling regime should now be divided into two, the early stage during which inverse Compton scattering dominates the total cooling and the late stage when it is unimportant compared with energy loss via synchrotron. Sections 4 and 5 discuss the observational consequences of the theory developed here. In § 4 we focus on how the physical interpretation of the observed spectral break frequencies and the time evolution of the afterglow emission must be modified to take into account the presence of extra cooling via inverse Compton scattering. In particular, we derive a useful physical limit on a combination of the observable parameters, measurements of which are generally the goal of afterglow observations. This result is then discussed in the context of GRB 970508.

[1] Chandra Fellow.

Finally, in § 5 we discuss the possibility of observing the inverse Compton (IC) emission directly. We show that the prospects of detecting this spectral component are very good for GRBs that explode in a medium with density of order 1 cm^{-3}. Our conclusions are summarized in § 6.

2. SPECTRUM

We make the standard assumption of a uniform magnetic field and a power-law injection of electrons, with the energy distribution given by $N(\gamma) \propto \gamma^{-p}$, behind the expanding shock front. Then the general shape of the afterglow spectrum is determined by the relationship between the electron cooling time and the system dynamical time. Below we consider two limiting cases: when the majority of the injected electrons can cool on the dynamical time of the system (fast cooling) or when the cooling affects only the electrons in the high-energy tail of the distribution (slow cooling).

2.1. *Slow Cooling*

In this case the electron energy distribution around the minimum injection energy, γ_m, is not affected by the cooling. However, electrons with Lorentz factors above some critical value, γ_c, radiate a significant fraction of their energy on the dynamical time. Since the ratio of the cooling time of an electron with Lorentz factor γ_e to the dynamical time is (γ_c/γ_e), the electron distribution above γ_c becomes steeper by one power of γ_e. Therefore, the resulting electron energy distribution is

$$N(\gamma) \propto \begin{cases} \gamma^{-p}, & \text{if} \quad \gamma_m < \gamma < \gamma_c, \\ \gamma^{-p-1}, & \text{if} \quad \gamma_c < \gamma. \end{cases} \tag{2.1}$$

As described by Sari et al. (1998), the synchrotron emission from such a distribution of electrons can be approximated by a broken power-law spectrum with three characteristic break frequencies. One is the self-absorption frequency, ν_a, below which the system becomes optically thick. The other two are the peak frequencies of the emission from the electrons with the characteristic Lorentz factors γ_m and γ_c, denoted ν_m and ν_c, respectively. Here we assume that ν_m and ν_c are greater than ν_a. At frequencies $\nu < \nu_a$, self-absorption is important and the specific flux is proportional to ν^2, while between ν_a and ν_m the synchrotron emission grows more slowly with $f \propto \nu^{1/3}$. The specific flux peaks at ν_m and then decreases as $\nu^{-(p-1)/2}$ for frequencies $\nu_m < \nu < \nu_c$; above ν_c it decreases as $\nu^{-p/2}$.

Using this synchrotron spectrum as the source of seed photons, we computed the resulting inverse Compton emission, by integrating over the differential scattering cross section and over the electron energy distribution given by equation (2.1) (this calculation is discussed in detail in Appendix A). We find that, like the original synchrotron spectrum, the upscattered component consists of four segments, with the breaks at three characteristic frequencies: $\nu_a^{\mathrm{IC}} \simeq 2\gamma_m^2 \nu_a$, $\nu_m^{\mathrm{IC}} \simeq 2\gamma_m^2 \nu_m$, and $\nu_c^{\mathrm{IC}} \simeq 2\gamma_c^2 \nu_c$. At frequencies $\nu < \nu_m^{\mathrm{IC}}$, the main contribution to the IC spectral component comes from synchrotron photons scattered by the electrons with Lorentz factor γ_m. In this region, the spectrum is well approximated by two power-law segments. The specific flux initially increases linearly with frequency up to ν_a^{IC}; this spectral slope is determined by the shape of the scattering cross section (see Appendix A). It then continues to rise as $\nu^{1/3}$ up to its peak at $\nu = \nu_m^{\mathrm{IC}}$.

In the frequency range $\nu_m^{\mathrm{IC}} < \nu < \nu_c^{\mathrm{IC}}$, electrons with a range of Lorentz factors between γ_m and γ_c contribute equally to the emission at each frequency. Because of this, the flux drops off roughly as $\nu^{-(p-1)/2}$, but with two major differences from the original synchrotron spectrum. First, the region with this spectral slope extends over double the frequency range (in logarithmic units) of the corresponding synchrotron component, i.e., $\nu_m^{\mathrm{IC}}/\nu_c^{\mathrm{IC}} = (\nu_m/\nu_c)^2$. Second, contributions from different electron energies generate a logarithmic term, which peaks at $\nu = (\nu_m^{\mathrm{IC}} \nu_c^{\mathrm{IC}})^{1/2}$, increasing the flux there by a factor of order $\ln(\nu_c/\nu_m)$ above that of the underlying power law (see eq. [A5]).

Similarly, at frequencies above ν_c^{IC}, the emission is composed of equal contributions from electrons with a range of Lorentz factors $\gamma_e > \gamma_c$. Here specific flux drops off as $\nu^{-p/2}$, but also with the addition of a logarithmically growing term of order $\ln(\nu/\nu_c^{\mathrm{IC}})$ (see eq. [A5]).

The inverse Compton spectral component, approximated as a broken power law and normalized using equation (2.3), below is shown in Figure 1*a* together with the more "exact" spectrum obtained by computing the integrals in equation (A2). To emphasize the importance of IC emission as a cooling mechanism, we plotted νf_ν versus ν, which gives a measure of energy emitted per logarithmic frequency interval. The comparison of the two curves shows that the power-law approximation does a very good job at frequencies below ν_m^{IC} but becomes somewhat inadequate at higher frequencies. In fact, our calculation shows that, at frequencies $\nu > \nu_m^{\mathrm{IC}}$, the spectrum of the IC emission has a continuously varying slope, without identifiable spectral breaks. Moreover, one must keep in mind that the observed IC spectral component is expected to be even smoother, since in our calculations we assumed a broken power-law distribution of the synchrotron seed photons and used a simplified description of the scattering cross section (see Appendix A).

Another feature of the detailed spectrum, which cannot be deduced from the power-law approximation, is that for small values of p the IC energy output actually peaks well above ν_c^{IC} (which is the peak emission frequency for the approximate power-law spectrum). It is easy to show that this feature is due to the presence of the logarithmic correction term. It persists for $2 < p \lesssim \sqrt{6}$, which includes the range of values deduced from observations (e.g., Wijers & Galama 1999; Sari, Piran, & Halpern 1999; Freedman & Waxman 2001).

2.2. *Fast Cooling*

In this regime all of the injected electrons are able to cool on the dynamical timescale of the afterglow. Therefore, there is a population of electrons with Lorentz factors below the injection minimum γ_m, and the resulting electron distribution takes the form

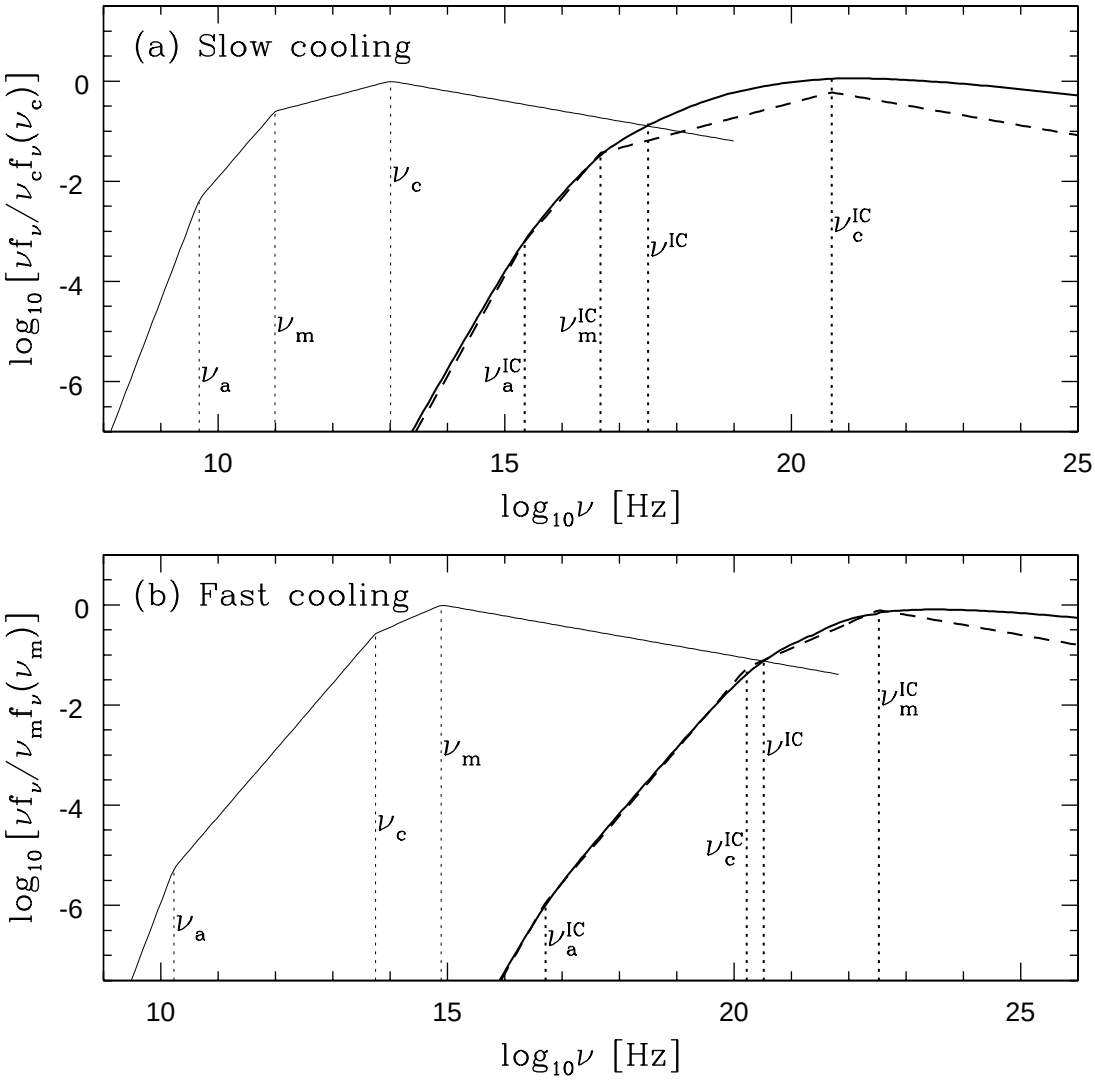

FIG. 1.—Total energy spectrum of a GRB afterglow, calculated using the following parameters: $p = 2.4$, $\epsilon_e = 0.5$, $\epsilon_B = 0.01$, $E_{52} = 0.5$, $z = 0.5$, $n_1 = 3$. The synchrotron component is shown as a thin solid line and the inverse Compton component as a thick solid line. A broken power-law approximation to the inverse Compton spectrum, normalized using eq. (2.3), is plotted as a dashed line for comparison. (*a*) Spectrum at $t = 12$ days, when the afterglow is in the slow-cooling regime. (*b*) Spectrum in the fast-cooling regime, computed for $t = 43$ minutes.

$$N(\gamma) \propto \begin{cases} \gamma^{-2}, & \text{if} \quad \gamma_c < \gamma < \gamma_m \,, \\ \gamma^{-p-1}, & \text{if} \quad \gamma_m < \gamma \,. \end{cases} \tag{2.2}$$

The synchrotron spectrum has the same three characteristic break frequencies, though now $\nu_c < \nu_m$, and consists of four power-law segments. Below ν_a the emission is optically thick and the specific flux increases as ν^2, and in the range $\nu_a < \nu < \nu_c$ we have $f_\nu \propto \nu^{1/3}$. The flux peaks at ν_c and declines as $f \propto \nu^{-1/2}$ for $\nu_c < \nu < \nu_m$ and as $f \propto \nu^{-p/2}$ above ν_m.

A spectrum of the inverse Compton emission in this regime is plotted in Figure 1*b*. Its general features are very similar to those of the slow-cooling case described above. The specific flux is linear in frequency below $\nu_a^{\rm IC}$ and continues as $f \propto \nu^{1/3}$ up to its peak at $\nu_c^{\rm IC}$; in the range $\nu_c^{\rm IC} < \nu < \nu_m^{\rm IC}$ it declines as $f \propto \nu^{-1/2}$ and drops off with $f \propto \nu^{-p/2}$ above $\nu_m^{\rm IC}$. Since most of the contribution to the IC emission below $\nu_c^{\rm IC}$ comes from the lowest energy electrons, a broken power law is a fairly good approximation to the spectrum in that region. At higher frequencies electrons with a range of Lorentz factors contribute to the emission, creating additional logarithmic terms (see eq. [A8]), which smooth out the breaks in the spectral slope.

2.3. *Peak Flux and Luminosity Ratios*

The strength of the inverse Compton emission relative to synchrotron can be estimated by considering the ratio of specific fluxes measured at the peak of the respective spectral components (peak of f_ν rather than νf_ν). We denote these peak fluxes as $f_{\rm max}$ and $f_{\rm max}^{\rm IC}$ for the synchrotron and inverse Compton components, respectively. As described in §§ 2.1 and 2.2 above, the former peaks at ν_m and the latter at $\nu_m^{\rm IC}$ in the slow-cooling regime and at ν_c and $\nu_c^{\rm IC}$, respectively, in the fast-cooling regime. In both cases the number of electrons that contribute to the radiation around the maximum is proportional to the total number

of electrons in the system, N. Therefore, the ratio of the two fluxes is simply

$$\frac{f_{\max}^{\rm IC}}{f_{\max}} \sim \frac{\sigma_T N}{4\pi R^2} \sim \frac{1}{3}\,\sigma_T nR = 2 \times 10^{-7} n_1 R_{18}\,, \tag{2.3}$$

where the last two terms assume that the electrons have been collected from an ambient medium with particle density $n = n_1 \times 1\ {\rm cm}^{-3}$ over a distance $R = R_{18} \times 10^{18}$ cm. For a range of values of n and R, which are relevant to the observable GRB afterglows, the flux ratio above is always much less than unity.

To assess the relative importance of contributions from the inverse Compton and synchrotron emission to the total cooling rate of the electrons, we can compute the ratio of the total energies emitted via these two mechanisms. Instead of integrating over the entire spectrum, we evaluate νf_ν at the peaks of the two spectral components and simply compute a ratio of the two values. Note that taking $L_{\rm syn} \sim \nu_c\, f_\nu(\nu_c)$ and $L_{\rm IC} \sim \nu_c^{\rm IC}\, f_\nu(\nu_c^{\rm IC})$ is not in general a good assumption, since direct spectral integration gives luminosities more than a factor of 10 greater than this estimate. However, since the shapes of the synchrotron and IC spectral components are similar, the correction factors nearly cancel out.

In the slow-cooling regime, the energy emitted via synchrotron peaks at ν_c. The inverse Compton emission can reach its maximum energy output at $\nu \gg \nu_c^{\rm IC}$ for small values of p (see § 2.1); however, since νf_ν is nearly flat in this region of the spectrum, for the purposes of this estimate we use $\nu_c^{\rm IC}\, f_\nu(\nu_c^{\rm IC})$. Then the luminosity ratio during the slow-cooling regime is

$$\frac{L_{\rm IC}}{L_{\rm syn}} \sim \frac{2}{3}\,\sigma_T nR\gamma_c^2 \left(\frac{\gamma_c}{\gamma_m}\right)^{1-p}. \tag{2.4}$$

In the fast-cooling regime the synchrotron and the IC energy emission peak at ν_m and $\nu_m^{\rm IC}$, respectively, and the luminosity ratio is given by

$$\frac{L_{\rm IC}}{L_{\rm syn}} \sim \frac{2}{3}\,\sigma_T nR\gamma_c\,\gamma_m\,. \tag{2.5}$$

3. AFTERGLOW EVOLUTION WITH STRONG COMPTON COOLING

Throughout most of the early afterglow evolution, inverse Compton emission typically dominates the total cooling rate, and therefore it determines the value of break energy in the electron energy distribution. This has a significant effect on the time evolution of both the synchrotron and the inverse Compton components.

3.1. *Luminosity Ratio*

The ratio of the inverse Compton to synchrotron luminosity can be computed in a more general way (Sari et al. 1996) that does not deal with the details of the spectrum but depends only on the underlying physical properties of the expanding shock wave. We generalize the derivation given by Sari et al. (1996) to describe both fast- and slow-cooling regimes by introducing a parameter η, equal to the fraction of the electron energy that was radiated away (via both synchrotron and IC emission). Then the ratio of luminosities, in the limit of single scattering, is given by

$$x \equiv \frac{L_{\rm IC}}{L_{\rm syn}} = \frac{U_{\rm rad}}{U_B} = \frac{U_{\rm syn}}{U_B} = \frac{\eta U_e/(1+x)}{U_B} = \frac{\eta\epsilon_e}{\epsilon_B(1+x)}\,, \tag{3.1}$$

where $U_{\rm syn}$, U_B, and U_e are the energy density of synchrotron radiation, magnetic field, and relativistic electrons, respectively. Note that in general $U_{\rm syn} = \eta\beta U_e/(1+x)$, where β is the velocity of material behind the shock front (in the frame of the shock); however, for a relativistic shock β is of order unity. The parameters ϵ_e and ϵ_B are defined as fractions of the total explosion energy that go into accelerating electrons and amplifying magnetic fields behind the shock front, respectively.

Solving equation (3.1) for x we obtain

$$x = \frac{-1 + \sqrt{1 + 4\eta\epsilon_e/\epsilon_B}}{2}\,. \tag{3.2}$$

This solution has two interesting limits:

$$x = \begin{cases} \dfrac{\eta\epsilon_e}{\epsilon_B}\,, & \text{if} \quad \dfrac{\eta\epsilon_e}{\epsilon_B} \ll 1\,, \\[2ex] \left(\dfrac{\eta\epsilon_e}{\epsilon_B}\right)^{1/2}\,, & \text{if} \quad \dfrac{\eta\epsilon_e}{\epsilon_B} \gg 1\,. \end{cases} \tag{3.3}$$

Hereafter, unless specified otherwise, we always use these approximate solutions for x.

Clearly, if $\eta\epsilon_e/\epsilon_B \ll 1$, the inverse Compton cooling rate is unimportant compared with synchrotron, and if $\eta\epsilon_e/\epsilon_B \gg 1$, it dominates the total emission. Using these expressions, the relative importance of IC emission can be evaluated using only the fundamental properties of the expanding shock and the ability of the electrons to cool. We can reduce this result to that in equations (2.4) and (2.5) above by noting that (1) for slow cooling $\eta = (\gamma_c/\gamma_m)^{2-p}$ and for fast cooling $\eta = 1$;

(2) $\gamma_m \sim \epsilon_e U/(m_e c^2 n)$, where U is the total energy density behind the shock; and (3) $\gamma_c \sim m_e c^2/(\sigma_T c \epsilon_B U t)$ if $\eta\epsilon_e/\epsilon_B \ll 1$, and $\gamma_c \sim m_e c^2/(x\sigma_T c \epsilon_B U t)$ if $\eta\epsilon_e/\epsilon_B \gg 1$.

3.2. *Effects on Synchrotron Spectrum and Light Curves*

Inverse Compton scattering can, in principle, affect the observed spectrum in three different ways (see also discussion in Sari et al. 1996). In the first place, it reduces the number of seed photons, changing the overall normalization of the synchrotron spectral component. This is important only if the Thompson optical depth is larger than unity and is therefore negligible in GRB afterglows. Second, IC scattering produces an additional emission component at higher frequencies, which we described in § 2. Finally, when the inverse Compton emission dominates the overall cooling of the electrons, it reduces the energy available for synchrotron radiation. Consequently, the cooling-break energy of the electron distribution, γ_c, is reduced from its standard (synchrotron only) value by a factor $(1 + x)$; i.e., in all our calculations we must replace $\gamma_c \rightarrow \gamma_c/(1 + x)$. It is the results of this latter effect that we discuss below.

From equation (3.3) it is clear that, if $\epsilon_e < \epsilon_B$, the IC power is never larger than the synchrotron power, since by definition $\eta \leq 1$. However, current estimates based on afterglow observations show that $\epsilon_B < \epsilon_e$; in fact in several objects the ratio ϵ_e/ϵ_B seems to be close to 100 (Wijers & Galama 1999; Granot, Piran, & Sari 1999). This implies that the magnetic field is relatively weak, and IC emission is important as long as $\eta \gtrsim 0.01$.

Assuming that $\epsilon_e > \epsilon_B$, the evolution of a GRB afterglow must now be divided into three regimes. In the first (fast-cooling) stage, most of the electron energy is lost, so that $\eta = 1$ and IC emission dominates over synchrotron by a time-constant factor $(\epsilon_e/\epsilon_B)^{1/2}$. Later, during the slow-cooling period, η decreases and so does the importance of IC scattering, though it still dominates the total cooling. Finally, η becomes so small that only synchrotron emission is important; this is the traditional slow-cooling regime. Below we discuss each of these stages in detail. Note that all our numerical results are computed in terms of $\epsilon_{B,-2} = \epsilon_B/0.01$ and $\epsilon_{e,0.5} = \epsilon_e/0.5$.

Since temporal evolution of the afterglow emission depends on the external density profile, the results are different in the case of the uniform ambient medium and the wind scenario, in which the density decreases as $\rho \propto r^{-2}$. We will present the results for the constant ambient density in this section and discuss the windlike density profile in Appendix B.

3.2.1. *Fast Cooling*

During the fast-cooling stage, IC scattering increases the radiation losses of each electron by a factor $1 + x \simeq x \simeq (\epsilon_e/\epsilon_B)^{1/2}$. Therefore, the cooling frequency $\nu_c \propto \gamma_c^2$ is reduced from its synchrotron-only value by a factor $x^2 \simeq \epsilon_e/\epsilon_B$. Moreover, since low-energy synchrotron emission is dominated by the electrons near the cooling break, the synchrotron self-absorption frequency increases by a factor $x \simeq (\epsilon_e/\epsilon_B)^{1/2}$. Because both ϵ_e and ϵ_B remain constant in time, these changes do not affect the time evolution of the synchrotron spectrum.

Since IC scattering increases the total cooling rate, it prolongs the duration of the fast-cooling regime. For a constant ambient density the transition to slow cooling is delayed by a factor ϵ_e/ϵ_B, if $\epsilon_e > \epsilon_B$. The correct transition time then becomes

$$t_0^{\rm IC} = 170(1 + z)\epsilon_e^3 \epsilon_B E_{52} n_1 \text{ days} = 6.3(1 + z)\epsilon_{e,0.5}^3 \epsilon_{B,-2} E_{52} n_1 \text{ hr}\,, \tag{3.4}$$

where $E = E_{52} \times 10^{52}$ ergs s^{-1} is the total energy of the explosion. By comparison, if $\epsilon_e/\epsilon_B < 1$, IC scattering is never an efficient cooling mechanism and we get the usual (synchrotron only) expression:

$$t_0 = 170(1 + z)\epsilon_e^2 \epsilon_B^2 E_{52} n_1 \text{ days}\,. \tag{3.5}$$

3.2.2. *Slow IC-dominated Cooling*

During the slow-cooling stage only the cooling frequency is affected by IC cooling. The parameter η is no longer equal to unity, so during this intermediate regime ν_c is reduced by a factor $(1 + x)^2 \simeq x^2 \simeq \eta\epsilon_e/\epsilon_B$, as long as $x > 1$. It is important to note that, though η decreases with time, its instantaneous value can be estimated directly from the observed synchrotron spectrum alone, since in the slow-cooling regime $\eta = (\gamma_c/\gamma_m)^{2-p} = (\nu_c/\nu_m)^{-(p-2)/2}$. Since the value of p is estimated to be in the range 2.2–2.4, the decrease of η is very slow and inverse Compton scattering remains a dominant cooling process for a long time.

Without inverse Compton cooling, $\nu_c \propto t^{-1/2}$ and $\nu_m \propto t^{-3/2}$ so that their ratio is $\nu_c/\nu_m = t/t_0$. Taking IC emission into account we have $\nu_c/\nu_m \simeq (t/t_0)x^{-2}$, and x evolves with time according to the following equation,

$$x = \sqrt{\frac{\eta\epsilon_e}{\epsilon_B}} = \left(\frac{\nu_c}{\nu_m}\right)^{-(p-2)/4} \sqrt{\frac{\epsilon_e}{\epsilon_B}} \simeq \left(\frac{t/t_0}{x^2}\right)^{-(p-2)/4} \sqrt{\frac{\epsilon_e}{\epsilon_B}}\,, \tag{3.6}$$

which gives

$$x \simeq \left(\frac{\epsilon_e}{\epsilon_B}\right)^{1/(4-p)} \left(\frac{t}{t_0}\right)^{-(p-2)/[2(4-p)]} = \sqrt{\frac{\epsilon_e}{\epsilon_B}} \left(\frac{t}{t_0^{\rm IC}}\right)^{-(p-2)/[2(4-p)]}\,. \tag{3.7}$$

One should keep in mind, however, that in deriving the equation above we used the relativistic time scalings for the frequency ratio ν_c/ν_m. Once the fireball is no longer relativistic, our basic expression for x (eq. [3.1]) is no longer valid. In the

nonrelativistic case x decreases as $t^{-3/10}$ for $p = 2$, and even more rapidly for larger p, considerably faster than implied in equation (3.7). Therefore, IC cooling ceases to be dominant shortly after the relativistic stage is over.

3.2.3. *Slow Synchrotron-dominated Cooling*

The third stage of afterglow evolution, when $x < 1$ and the IC cooling rate is weaker than the synchrotron cooling rate and therefore has no effect on the synchrotron spectrum, begins at time

$$t^{\rm IC} = t_0^{\rm IC}\left(\frac{\epsilon_e}{\epsilon_B}\right)^{(4-p)/(p-2)} = 3\ {\rm yr}\left(\frac{\epsilon_{e,0.5}}{\epsilon_{B,-2}}\right)^{(4-p)/(p-2)} \epsilon_{e,0.5}^3\,\epsilon_{B,-2}\,E_{52}\,n_1\ , \tag{3.8}$$

with the numerical coefficient computed for $p = 2.3$. Note that this expression is very sensitive to the value of p and goes to infinity when $p \to 2$.

Equation (3.8) implies that, for $\epsilon_e/\epsilon_B \gtrsim 10$, the IC scattering dominates total cooling over the whole relativistic stage of afterglow evolution and, therefore, over the time period containing most current observations.

3.3. *Inverse Compton Light Curves*

Equations describing light curves of inverse Compton emission in the regimes of fast cooling and slow cooling with negligible IC (as defined in §§ 3.2.1 and 3.2.3) were given in Panaitescu & Kumar (2000), so we omit them here. One must keep in mind, however, that these equations were derived using the broken power-law approximation to the IC spectral component and so must be used with caution. During the intermediate stage (see § 3.2.2), when $\nu_c > \nu_m$ but the total cooling rate is dominated by IC scattering, the break frequencies of the IC spectral component and its peak flux evolve with time in the following way:

$$\begin{aligned} &\nu_a^{\rm IC} = 2\gamma_m^2\,\nu_a \propto t^{-3/4}\ , \qquad \nu_m^{\rm IC} = 2\gamma_m^2\,\nu_m \propto t^{-9/4}\ , \\ &\nu_c^{\rm IC} = 2\gamma_c^2\,\nu_c \propto (1+x)^{-4}t^{-1/4} \propto t^{-1/4+[2(p-2)]/(4-p)}\ , \qquad f_m^{\rm IC} \sim \sigma_T\,Rnf_m \propto t^{1/4}\ . \end{aligned} \tag{3.9}$$

For a range of values of p consistent with constraints from observations, the break frequency $\nu_c^{\rm IC}$ remains nearly constant or increases with time: $\nu_c^{\rm IC} \propto t^{-0.03}$ for $p = 2.2$ and $\nu_c^{\rm IC} \propto t^{0.25}$ for $p = 2.4$. It is therefore unlikely that it can ever be observed directly with X-ray instruments (see Fig. 1).

Using the expressions above and the detailed spectrum described in Appendix A, one can obtain the light curve of the IC emission at any frequency. As we emphasized earlier, taking only the broken power-law approximation to the IC spectrum can miss considerably and can be used only to get a very rough estimate, given below:

$$f_\nu^{\rm IC} \propto \begin{cases} t^{9/4}\ , & \text{if}\quad \nu < \nu_a^{\rm IC}\ , \\ t^{1}\ , & \text{if}\quad \nu_a^{\rm IC} < \nu < \nu_m^{\rm IC}\ , \\ t^{-(9p-11)/8}\ , & \text{if}\quad \nu_m^{\rm IC} < \nu < \nu_c^{\rm IC}\ , \\ t^{-(9p-10)/8+(p-2)/(4-p)}\ , & \text{if}\quad \nu_c^{\rm IC} < \nu\ . \end{cases} \tag{3.10}$$

The equation above differs from that given by Panaitescu & Kumar above the frequency $\nu_c^{\rm IC}$. Their expression is valid only at late times, when IC cooling is not important, while equation (3.10) is valid during the intermediate stage of afterglow evolution (slow cooling dominated by IC). As we stressed earlier, for typical GRB parameters, this intermediate stage lasts throughout the relativistic evolution of the fireball.

4. INFERRING AFTERGLOW PARAMETERS FROM THE SYNCHROTRON SPECTRAL COMPONENT

Even if the IC emission is not directly observed, its presence affects how we interpret the properties of the observable synchrotron spectral component. The general shape of the synchrotron emission is not affected by the IC scattering. However, when this extra source of cooling is taken into account, it lowers the predicted value of the cooling frequency, ν_c, by a factor $(1 + x)^2$. In addition to this, since during the fast-cooling stage the self-absorption frequency, ν_a, depends on the cooling frequency, in this regime its value increases by a factor $(1 + x)$. The resulting modified expressions for the break frequencies and the peak flux of the synchrotron spectrum are listed below:

$$\nu_a^{\rm slow} = 3.6\ {\rm GHz}\ (1+z)^{-1}\epsilon_{e,0.5}^{-1}\,\epsilon_{B,-2}^{1/5}\,E_{52}^{1/5}\,n_1^{3/5}\ , \tag{4.1}$$

$$\nu_a^{\rm fast} = 0.15\ {\rm GHz}\ (1+z)^{-1/2}\epsilon_{B,-2}^{6/5}\,E_{52}^{7/10}\,n_1^{11/10}t_{\rm day}^{-1/2}(1+x)\ , \tag{4.2}$$

$$\nu_m = 5\times 10^{12}\ {\rm Hz}\ (1+z)^{1/2}\epsilon_{B,-2}^{1/2}\,\epsilon_{e,0.5}^{2}\,E_{52}^{1/2}\,t_{\rm day}^{-3/2}\ , \tag{4.3}$$

$$\nu_c = 2.7\times 10^{15}\ {\rm Hz}\ (1+z)^{-1/2}\epsilon_{B,-2}^{-3/2}\,E_{52}^{-1/2}\,n_1^{-1}t_{\rm day}^{-1/2}(1+x)^{-2}\ , \tag{4.4}$$

$$f_{\rm max} = 2.6\ {\rm mJy}\ (1+z)\epsilon_{B,-2}^{1/2}\,E_{52}\,n_1^{1/2}\,D_{L,28}^{-2}\ , \tag{4.5}$$

where $D_{L,28}$ is the luminosity distance in units of 10^{28} cm. The coefficients in these equations were taken from the synchrotron spectrum calculation of Granot et al. (1999) and are somewhat dependent on p. The numerical values here are quoted for

$p = 2.2$. To compute full expressions for the IC break frequencies and peak flux (eq. 3.9) one should use eqs. (4.1)–(4.5) together with

$$\gamma_m = 930\epsilon_{e,0.5}(E_{52}/n_1)^{1/8}t_{\rm day}^{-3/8}\ , \tag{4.6}$$

$$\gamma_c = \gamma_m(\nu_c/\nu_m)^{1/2}\ , \tag{4.7}$$

$$R = 3.9 \times 10^{17}(E_{52}/n_1)^{1/4}t_{\rm day}^{1/4}\ . \tag{4.8}$$

Combining equations (3.1) and (4.1)–(4.5), we can now derive an interesting constraint on the observable afterglow parameters:

$$C \equiv 0.06(1+z)^4 t_{\rm day}^4 D_{L,28}^{-2}\eta\left(\frac{\nu_a}{\rm GHz}\right)^{10/3}\left(\frac{\nu_m}{10^{13}\ {\rm Hz}}\right)^{13/6}\left(\frac{\nu_c}{10^{14}\ {\rm Hz}}\right)^{3/2}\left(\frac{F_{\nu_m}}{\rm mJy}\right)^{-1} = \frac{x}{(1+x)^2}\ . \tag{4.9}$$

The expression on the right-hand side has a maximum value of $\frac{1}{4}$. Thus, equation (4.9) above gives us a theoretical constraint on this combination of the observed break frequencies and peak flux for any afterglow spectrum, completely independent of its underlying physical parameters! Note that η is also an observable quantity, since it is given by $\eta = \min\,[(\nu_c/\nu_m)^{(2-p)/2}, 1]$. The only assumption made in deriving this constraint is that we are seeing the synchrotron emission from a power-law distribution of electrons accelerated by a relativistic shock wave.

For fast cooling, we can write a similar combination. It is simpler, however, to use the same combination C as above, in which we substitute the "adjusted" frequency given by

$$\nu_a^{\rm slow} = \nu_a^{\rm fast}\left(\frac{\nu_c}{\nu_m}\right)^{1/2} \tag{4.10}$$

instead of the observed self-absorption frequency $\nu_a^{\rm fast}$.

To illustrate how this constraint can be used, let us consider GRB 970508, which has probably the best-studied afterglow to date. Galama et al. (1998) described the observed broadband spectrum of that burst and have shown it to be in good agreement with the synchrotron spectrum of Sari et al. (1998). Their fit shows that at $t = 12.1$ days $\nu_c \cong 1.6 \times 10^{14}$ Hz, $\nu_m \cong 8.6 \times 10^{10}$ Hz, $\nu_a \cong 3.1$ GHz, and $f_{\rm max} = 1.7$ mJy and $p \cong 2.2$. Using the break frequencies of GRB 970508 as given by Galama et al. (1998), we see that equation (4.9) gives $C \cong 4 \gg \frac{1}{4}$. Though this result seems to suggest that the observed spectrum could not be produced by synchrotron emission, a more likely explanation is that the values of the break frequencies are not accurate. Both ν_m and ν_c are rather weakly constrained by the observations, and a factor of a few could easily resolve this disagreement.

We recommend the following procedure to determine the afterglow parameters from a snapshot of the spectrum. First, one calculates the combinations of observables, C, as given in equation (4.9) (with the correction of eq. [4.10], if $\nu_c < \nu_a$). If $C > \frac{1}{4}$, then there is no consistent solution. If $C < \frac{1}{4}$, there are two solutions, which can be found in the following way. First we solve equation (4.9) to give the two possible values of x:

$$x_1 = \frac{1 - 2C - \sqrt{1-4C}}{2C} \cong C \ll 1 \tag{4.11}$$

and

$$x_2 = \frac{1 - 2C + \sqrt{1-4C}}{2C} \cong \frac{1}{C} \gg 1\ . \tag{4.12}$$

The two solutions for the physical parameters describing the afterglow are then given by

$$E_{52} = 0.23\left(\frac{\nu_a}{\rm GHz}\right)^{-5/6}\left(\frac{\nu_m}{10^{13}\ {\rm Hz}}\right)^{-5/12}\left(\frac{\nu_c}{10^{14}\ {\rm Hz}}\right)^{1/4}\left(\frac{F_{\nu_m}}{\rm mJy}\right)^{3/2} t_{\rm day}^{-1/2}(1+z)^{-2}D_{L,28}^3(1+x)^{1/2}\ , \tag{4.13}$$

$$\epsilon_e = 0.23\left(\frac{\nu_a}{\rm GHz}\right)^{5/6}\left(\frac{\nu_m}{10^{13}\ {\rm Hz}}\right)^{11/12}\left(\frac{\nu_c}{10^{14}\ {\rm Hz}}\right)^{1/4}\left(\frac{F_{\nu_m}}{\rm mJy}\right)^{-1/2} t_{\rm day}^{3/2}(1+z)D_{L,28}^{-1}(1+x)^{1/2}\ , \tag{4.14}$$

$$\epsilon_B = 3.9\left(\frac{\nu_a}{\rm GHz}\right)^{-5/2}\left(\frac{\nu_m}{10^{13}\ {\rm Hz}}\right)^{-5/4}\left(\frac{\nu_c}{10^{14}\ {\rm Hz}}\right)^{-5/4}\left(\frac{F_{\nu_m}}{\rm mJy}\right)^{1/2} t_{\rm day}^{-5/2}(1+z)^{-3}D_{L,28}(1+x)^{-5/2}\ , \tag{4.15}$$

$$n_1 = 0.0072\left(\frac{\nu_a}{\rm GHz}\right)^{25/6}\left(\frac{\nu_m}{10^{13}\ {\rm Hz}}\right)^{25/12}\left(\frac{\nu_c}{10^{14}\ {\rm Hz}}\right)^{3/4}\left(\frac{F_{\nu_m}}{\rm mJy}\right)^{-3/2} t_{\rm day}^{7/2}(1+z)^5 D_{L,28}^{-3}(1+x)^{3/2}\ . \tag{4.16}$$

Since $1 + x_1 \cong 1$, one of these solutions degenerates to that given in Wijers & Galama (1999) with the corrected coefficients of Granot et al. (1999). However, in the second case we have $x_2 \gg 1$ so that the resulting values of E_{52}, ϵ_e, ϵ_B, and n_1 are

significantly different. Substituting $1 + x_2 \sim x_2 \sim 1/C$ in these equations we obtain

$$E_{52} = 0.95\eta^{-1/2}\left(\frac{\nu_a}{\mathrm{GHz}}\right)^{-5/2}\left(\frac{\nu_m}{10^{13}\ \mathrm{Hz}}\right)^{-3/2}\left(\frac{\nu_c}{10^{14}\ \mathrm{Hz}}\right)^{-1/2}\left(\frac{F_{\nu_m}}{\mathrm{mJy}}\right)^{2} t_{\mathrm{day}}^{-5/2}(1+z)^{-4}D_{L,28}^{4}\ , \tag{4.17}$$

$$\epsilon_e = 0.95\eta^{-1/2}\left(\frac{\nu_a}{\mathrm{GHz}}\right)^{-5/6}\left(\frac{\nu_m}{10^{13}\ \mathrm{Hz}}\right)^{-1/6}\left(\frac{\nu_c}{10^{14}\ \mathrm{Hz}}\right)^{-1/2} t_{\mathrm{day}}^{-1/2}(1+z)^{-1}\ , \tag{4.18}$$

$$\epsilon_B = 0.0032\eta^{5/2}\left(\frac{\nu_a}{\mathrm{GHz}}\right)^{35/6}\left(\frac{\nu_m}{10^{13}\ \mathrm{Hz}}\right)^{25/6}\left(\frac{\nu_c}{10^{14}\ \mathrm{Hz}}\right)^{5/2}\left(\frac{F_{\nu_m}}{\mathrm{mJy}}\right)^{-2} t_{\mathrm{day}}^{15/2}(1+z)^{7}D_{L,28}^{-4}\ , \tag{4.19}$$

$$n_1 = 0.51\eta^{-3/2}\left(\frac{\nu_a}{\mathrm{GHz}}\right)^{-5/6}\left(\frac{\nu_m}{10^{13}\ \mathrm{Hz}}\right)^{-7/6}\left(\frac{\nu_c}{10^{14}\ \mathrm{Hz}}\right)^{-3/2} t_{\mathrm{day}}^{-5/2}(1+z)^{-1}\ . \tag{4.20}$$

This second solution, where IC dominates, was neglected so far. It has a somewhat higher energy, higher density, higher ϵ_e, and lower ϵ_B than the low-x solution.

How can we determine which of the two solutions is correct at a given moment? This cannot be done by studying a single snapshot of the afterglow spectrum. However, the temporal evolution above the cooling frequency is a little different in the two cases. The decay rate is slower in the second, IC-dominated, solution. If the decay rates below and above the cooling frequency are measured to be $t^{-\alpha_1}$ and $t^{-\alpha_2}$, respectively, then (for constant density of ambient material) the standard model, which ignores IC emission, predicts $\alpha_2 - \alpha_1 = \frac{1}{4}$. The presence of strong IC cooling will make the difference smaller, giving $\alpha_2 - \alpha_1 = \frac{1}{4} - (p-2)/(8-2p) \cong 0.2$. For a windlike ambient density profile (see Appendix B), the standard model predicts $\alpha_2 - \alpha_1 = -\frac{1}{4}$, which changes to $\alpha_2 - \alpha_1 = -\frac{1}{4} - (p-2)/(4-p) \cong -0.36$ when the IC emission dominates the cooling. This difference is not large (except perhaps in the wind model), and therefore an accurate measurement with long temporal baselines is needed.

It was recently argued by Freedman & Waxman (2001) that the total energy contained in the electrons behind the shock $\epsilon_e E$ can be estimated using a single observation above the cooling frequency. They argued that this is insensitive to the value of the magnetic field. Their analysis, which ignores IC, could be explained as follows. Since the electron energy distribution is flat, i.e., $p \sim 2$, each decade in the electron distribution contains an amount of energy of the order of the total energy in all the electrons. Above the cooling frequency all of this energy is radiated, and therefore the observed νF_ν gives an approximate measure of the total electron energy. However, we have shown that, if the ratio (ϵ_e/ϵ_B) is large, most of this energy is radiated as IC emission rather than synchrotron. Therefore, during the fast-cooling stage the energy estimate suggested by Freedman & Waxman (2001) falls short of $\epsilon_e E$ by a factor $(\epsilon_e/\epsilon_B)^{1/2}$ while during the intermediate stage it is short by a factor $(\eta\epsilon_e/\epsilon_B)^{1/2}$, which is roughly proportional to $\epsilon_B^{-0.45}$, and both of these correction factors depend on the magnetic field. Thus, the Freedman & Waxman (2001) method can provide only a lower limit on $\epsilon_e E$.

5. DIRECT DETECTION OF IC EMISSION

Clearly, the IC emission component can be detected directly only at frequencies where it dominates the synchrotron emission. As can be seen from Figure 1, for typical parameters this occurs in the X-ray and γ-ray bands. Here we limit our discussion to the intermediate regime (defined in § 3.2.2) of afterglow evolution, during which the crossing point between the synchrotron and IC spectral components, ν^{IC}, generally lies above the synchrotron cooling frequency ν_c and between IC break frequencies ν_a^{IC} and ν_c^{IC}. Using the power-law approximation for both spectral components it is then straightforward to compute ν^{IC}, both at early times, when $\nu^{\mathrm{IC}} < \nu_m^{\mathrm{IC}}$, and at later times, when $\nu^{\mathrm{IC}} > \nu_m^{\mathrm{IC}}$. We obtain the following expressions:

$$\nu^{\mathrm{IC}} = \begin{cases} \nu_m^{\mathrm{IC}}\left[\dfrac{\epsilon_B}{\epsilon_e}\left(\dfrac{\gamma_c}{\gamma_m}\right)^4 (2\gamma_m\gamma_c)^{2-p}\right]^{3/(2+3p)} \propto t^{3(3p^2-8p-12)/[2(2+3p)(4-p)]}, & \text{if } \nu^{\mathrm{IC}} < \nu_m^{\mathrm{IC}}; \\ \nu_c^{\mathrm{IC}}\dfrac{\epsilon_B}{\epsilon_e}(2\gamma_m\gamma_c)^{2-p} \propto t^{(3p^2-23p+36)/[4(p-4)]}, & \text{if } \nu^{\mathrm{IC}} > \nu_m^{\mathrm{IC}}. \end{cases} \tag{5.1}$$

It is easy to show that the transition between these two regimes occurs when $\gamma_c/\gamma_m \simeq [(\epsilon_e/\epsilon_B)\gamma_m^{2(p-2)}]^{1/(6-p)}$. Note that it is not necessary to know a priori which regime is relevant in a given case. One can simply compute ν^{IC} using both expressions given above and then take the larger value, which will always be the correct one.

To determine whether direct observations of the IC emission are feasible, it is best to write ν^{IC} in terms of the underlying physical parameters describing GRB afterglow. We give the expression for two characteristic values of p. For $p = 2.2$ (and uniform-density ambient medium), we obtain

$$\nu^{\mathrm{IC}} = \max\left[2.6\times10^{19}\epsilon_{e,0.5}^{1.3}\epsilon_{B,-2}^{0.1}n_1^{-1}t_{\mathrm{day}}^{-1.5}(1+z)^{0.5}\ ;\quad 2.1\times10^{20}E_{52}^{-1.4}\epsilon_{e,0.5}^{-3.7}\epsilon_{B,-2}^{-0.6}n_1^{-2.3}(1+z)^{-1}\right]\ \mathrm{Hz}\ , \tag{5.2}$$

while for $p = 2.4$ we get

$$\nu^{\mathrm{IC}} = \max\left[1.3\times10^{19}\epsilon_{e,0.5}^{1.2}\epsilon_{B,-2}^{0.1}n_1^{-1}t_{\mathrm{day}}^{-1.4}(1+z)^{0.4}\ ;\quad 3.1\times10^{18}E_{52}^{-1.6}\epsilon_{e,0.5}^{-4.5}\epsilon_{B,-2}^{-0.75}n_1^{-2.4}t_{\mathrm{day}}^{0.3}(1+z)^{-1.3}\right]\ \mathrm{Hz}\ . \tag{5.3}$$

The first and second expressions in parentheses describe early- and late-time evolution of ν^{IC}, respectively. The dependence on p is small as long as $\nu^{\mathrm{IC}} < \nu_m^{\mathrm{IC}}$. However, if $\nu^{\mathrm{IC}} > \nu_m^{\mathrm{IC}}$, the sensitivity to p is large (because we are calculating the intersection point of two almost parallel lines). For the same reason, when the latter expression applies, it may considerably overestimate (perhaps by more than 1 order of magnitude) the value of ν^{IC}, since it is based on an approximate power-law description of the

IC spectrum, which underestimates the IC flux (see Fig. 1). In both cases it seems that the uncertainties in our formalism are larger than those introduced by the p dependence. A graph of $\nu^{\rm IC}$ as a function of time is given in Figure 2. The graphs are done using both the power-law approximates (eqs. [5.2] and [5.3]) and the more exact IC spectrum of Figure 1. It is evident that the power-law approximation is reasonable at early times (when $\nu^{\rm IC} < \nu_m^{\rm IC}$) and is an overestimate of $\nu^{\rm IC}$ by more than 1 order of magnitude at late times. This discrepancy stresses again the poor quality of the power-law approximation.

From equations (5.2) and (5.3) it is clear that $\nu^{\rm IC}$ reaches its minimum values at a time when $\nu^{\rm IC} = \nu_m^{\rm IC}$. (Using eq. [5.1] it can easily be shown that this is a general property of the transition frequency, as long as $p \gtrsim 2.2$.) Since both *Chandra* and *XMM* cannot observe hard X-rays, the IC component can be seen directly only while, say, $\nu^{\rm IC} \lesssim 5$ keV. This condition places a lower limit on the ambient density. For $p = 2.2$, we need $n_1 \gtrsim 3.5 E_{52}^{-0.6} \epsilon_{e,0.5}^{-1.6} \epsilon_{B,-2}^{-0.26} (1+z)^{-0.4}$, while for $p = 2.4$ we should have $n_1 \gtrsim 1.4 E_{52}^{-0.6} \epsilon_{e,0.5}^{-1.7} \epsilon_{B,-2}^{-0.27} (1+z)^{-0.5}$, in general agreement with Panaitescu & Kumar (2000). In the above estimates for the required density we have taken into account the overestimate of equations (5.2) and (5.3).

If the ambient density is high enough to satisfy the above conditions, then the following sequence of events should be observed in X-rays near 5 keV. The X-ray flux begins to be dominated by IC emission at time $t \sim 7.7$ days $\epsilon_{e,0.5}^{0.9} \epsilon_{B,-2}^{0.08} n_1^{-0.7} (1+z)^{0.3}$ for $p = 2.2$ and $t \sim 5.5$ days $\epsilon_{e,0.5}^{0.9} \epsilon_{B,-2}^{0.07} n_1^{-0.7} (1+z)^{0.3}$ for $p = 2.4$, causing the observed spectral slope to change from $-p/2$ to $\frac{1}{3}$. After the transition, the IC flux increases linearly with time (eq. [3.10]), producing a bump in the X-ray light curve (see also Fig. 3 of Panaitescu & Kumar 2000).

The observed flux peaks when $\nu_m^{\rm IC}$ moves into the X-ray band at time $t \sim 3.2$ days $E_{52}^{1/3} \epsilon_{e,0.5}^{16/9} \epsilon_{B,-2}^{2/9} n_1^{-1/9} (1+z)^{5/9}$ (independent of p). At the same time the spectral slope begins to change gradually from $\frac{1}{3}$ to $-(p-1)/2$, which is still easily distinguishable from the characteristic $-p/2$ slope of the synchrotron high-energy tail. From this point on, the observed flux evolves as

$$f_\nu^{\rm IC} \sim 4.4 \times 10^{-15} \left(\frac{\nu}{5\ {\rm keV}}\right)^{-0.6} E_{52}^{1.7} \epsilon_{e,0.5}^{2.4} \epsilon_{B,-2}^{0.8} n_1^{1.1} D_{L,28}^{-2} (1+z)^{1.5} t_{\rm day}^{-1.1}\ {\rm ergs\ (s\ cm^2\ keV)^{-1}} \tag{5.4}$$

for $p = 2.2$ and as

$$f_\nu^{\rm IC} \sim 1.1 \times 10^{-14} \left(\frac{\nu}{5\ {\rm keV}}\right)^{-0.7} E_{52}^{1.8} \epsilon_{e,0.5}^{2.8} \epsilon_{B,-2}^{0.9} n_1^{1.1} D_{L,28}^{-2} (1+z)^{1.6} t_{\rm day}^{-1.3}\ {\rm ergs\ (s\ cm^2\ keV)^{-1}} \tag{5.5}$$

for $p = 2.4$. For comparison, the Advanced CCD Imaging Spectrometer (ACIS) on *Chandra* can detect fluxes down to 4×10^{-15} ergs s^{-1} cm^{-2} (in the energy band 0.4–6 keV) in a 10^4 s observation. Thus, for reasonable values of the afterglow parameters, the IC emission should be observable. Specifically, if E_{52} is somewhat larger than unity (as is the case for a

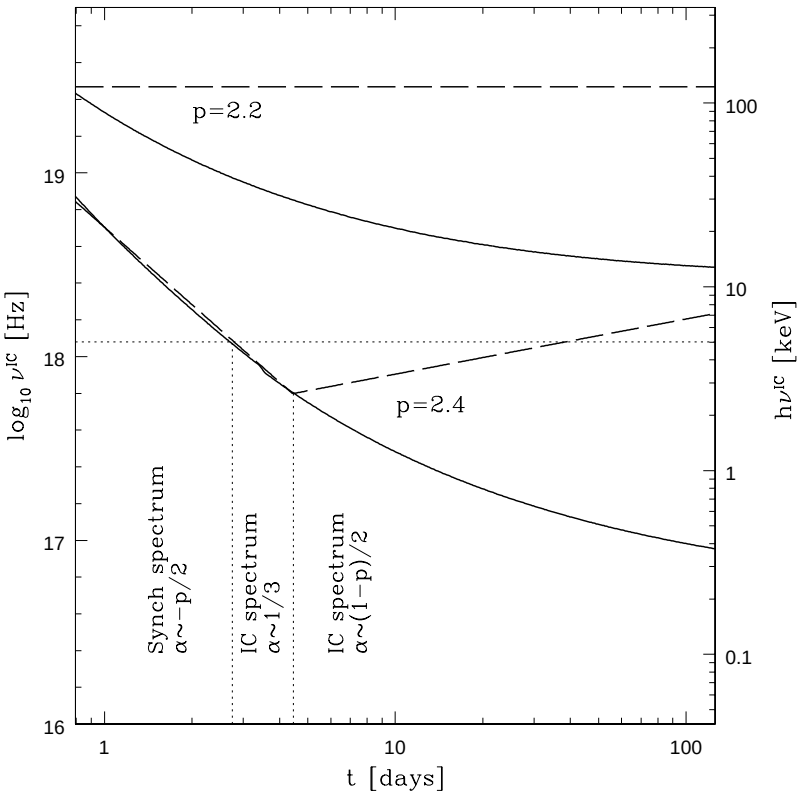

FIG. 2.—Frequency above which IC dominates the emission, as a function of time, for $p = 2.2$ and $p = 2.4$ using $\epsilon_e = 0.5$, $\epsilon_B = 0.01$, $E_{52} = 0.5$, $z = 0.5$, $n_1 = 3$. Dashed lines show $\nu^{\rm IC}$ calculated using the power-law approximation for the IC spectrum, while the solid lines give the result computed using the exact spectrum (see Fig. 1). For the case of $p = 2.4$, three temporal domains of the X-ray flux behavior are indicated. At early times the X-ray flux is dominated by synchrotron with spectral slope of $\nu^{-p/2}$. Later, when the X-ray emission is dominated by IC the observed flux first rises and has a spectral slope of $\nu^{1/3}$ and then, when $\nu_m^{\rm IC}$ drops below the X-ray band, the flux decreases and has a spectral slope of about $\nu^{-(p-1)/2}$.

reasonable fraction of the bursts) and if the density is somewhat higher than unity (as is required for IC emission to dominate the observed X-ray flux), then the inverse Compton emission should stay visible for several weeks or even months.

6. SUMMARY

In this paper we calculate the detailed spectrum of the inverse Compton emission from a relativistic shock in the context of GRB afterglows. The general shape of this spectral component is very similar to the primary synchrotron spectrum. Like the latter, the spectrum of the IC emission can be roughly approximated by a broken power law with break frequencies $\nu_a^{\rm IC}$, $\nu_m^{\rm IC}$, and $\nu_c^{\rm IC}$ (defined in § 2.1). However, it differs from the synchrotron spectral component on three major points, summarized below. (1) At the low-frequency end of the spectrum, $\nu < \nu_a^{\rm IC}$, the emission increases as $\propto \nu$, rather than as $\propto \nu^2$, characteristic of the synchrotron spectrum below ν_a. This may not have major practical consequences, however, since the low-frequency part of the IC spectral component is generally obscured by the synchrotron high-energy tail. (2) The part of the IC spectrum that lies between $\nu_c^{\rm IC}$ and $\nu_m^{\rm IC}$ extends over twice as many decades as the corresponding region (between ν_m and ν_c) in the synchrotron spectrum. (3) The segments of the IC spectral component above the peak frequency ($\nu_m^{\rm IC}$ in the slow-cooling regime and above $\nu_c^{\rm IC}$ in the fast-cooling regime) cannot be well described by the pure power-law terms. The presence of additional logarithmic terms in this frequency range has the effect of considerably smoothing out the spectral breaks. Thus, no sharp changes in the spectral slope or in the rate of time evolution are expected during the observation of the IC emission above the peak frequency. In contrast, the observed transition between the synchrotron and Compton components can be sharp and produce quite dramatic spectral and temporal changes.

In § 3.1 we give a simple prescription for estimating the importance of IC emission for the total cooling rate of the shocked gas. We showed that, if the fraction of energy contained in relativistic electrons, ϵ_e, is larger than that in the magnetic field, ϵ_B, then, during the fast-cooling stage, IC emission is greater than the emission due to synchrotron by a factor of $(\epsilon_e/\epsilon_B)^{1/2}$. This factor decreases very slowly in the slow-cooling regime, since at any given moment electrons located high enough in the power-law distribution are always cooling. Since the electron distribution is close to being flat, these electrons can still radiate a significant fraction of the total electron energy. Thus, the afterglow evolution during the early part of the slow-cooling regime is also dominated by IC emission. Moreover, we found that, for $\epsilon_e/\epsilon_B > 10$, the IC scattering is likely to remain the dominant cooling mechanism throughout the entire relativistic stage.

As long as the IC emission dominates the total cooling rate, it sets the energy of the cooling break, γ_c, in the electron energy distribution and determines the cooling frequency of the synchrotron spectral component. Therefore, the presence of IC emission changes the values of physical parameters inferred from current afterglow observations. In § 4 we give the revised prescription for computing the total explosion energy, E, the fractions of energy in electrons and magnetic fields, ϵ_e and ϵ_B, and the ambient particle density, n, using the observed properties of the synchrotron spectral component. We show that at any instance in time two possible solutions for E, ϵ_e, ϵ_B, and n are allowed, one where IC cooling is unimportant and another where it dominates the total emission from the afterglow. There is no way to distinguish between the two solutions based on an instantaneous synchrotron spectrum alone. They differ only in their time evolution of emission above ν_c and in the strength of the IC spectral component.

We also obtain an important constraint on the instantaneous values of the synchrotron break frequencies, peak flux of the synchrotron component, and the redshift of the afterglow in the slow-cooling regime. We show that, because of the presence of the IC cooling rate, the combination of these parameters must always be smaller than $\frac{1}{4}$.

Finally, we discuss the possibility of detecting the IC emission component directly. We show that, for reasonable values of the physical parameters, this component can be detected by *Chandra* a few days after the initial burst, as long as the ambient density is greater than $\sim 1\ {\rm cm}^{-3}$. Whether or not the IC component is detected will be apparent from the change in observed spectral slope, as well as from the bump in the X-ray light curve.

R. S. gratefully acknowledges support from the Sherman Fairchild foundations. A. E. was supported by NASA through Chandra Postdoctoral Fellowship grant PF8-10002 awarded by the Chandra X-Ray Center, which is operated by the SAO for NASA under contract NAS8-39073.

APPENDIX A

DETAILS OF COMPTON SCATTERING

The Thomson optical depth through the shocked medium, $\tau \sim \sigma_T nR$, is generally very small, of order 10^{-6}. In this case the Compton y-parameter, $y = \gamma_e^2 \tau$, determines the average fractional energy change of seed photons in each scattering by an electron with Lorentz factor γ_e. When $y < 1$, only single scattering needs to be considered in computing inverse Compton emission. When $y > 1$, multiple scattering can be important. However, in the context of GRB afterglows, a once-scattered synchrotron photon with initial energy $h\nu$ generally has energy of order $\gamma_e^3 h\nu \gtrsim m_e c^2$ in the rest frame of the second scattering electron. Then the Thomson limit no longer applies and the energy gain in each successive scattering will be reduced because of electron recoil and the necessity of using the Klein-Nishina scattering cross section. We conclude, therefore, that multiple scattering of synchrotron photons can be ignored.

For single scattering, the inverse Compton volume emissivity for a power-law distribution of scattering electrons is given by (Rybicki & Lightman 1979)

$$j_\nu^{\rm IC} = 3\sigma_T \int_{\gamma_m}^{\infty} d\gamma N(\gamma) \int_0^1 dx\, g(x) \tilde{f}_{\nu_s}(x)\ , \tag{A1}$$

where $x \equiv \nu/4\gamma^2\nu_s$, $\tilde{f}_{\nu_s}$ is the incident specific flux at the shock front, and $g(x) = 1 + x + 2x\ln x - 2x^2$ takes care of the angular dependence of the scattering cross section in the limit $\gamma \gg 1$ (Blumenthal & Gould 1970). However, the quantities that are easiest to compare with the observations are the flux in the inverse Compton component, $f_\nu^{\rm IC} = j_\nu^{\rm IC}(4/3)R^3/(4\pi D^2)$, and the synchrotron flux, $f_{\nu_s} = \tilde{f}_{\nu_s} 4\pi R^2/(4\pi D^2)$, where R is the size of the shocked region and D is the distance to the observer. Strictly speaking, both j and $\tilde{f}$ are measured in the rest frame of the shocked medium, but they transform in the same way to the observer's frame, so the transformation factors cancel each other out (as do redshift effects). Substituting these quantities into equation (A1) gives us

$$f_\nu^{\rm IC} = R\sigma_T \int_{\gamma_m}^{\infty} d\gamma N(\gamma) \int_0^{x_0} dx f_{\nu_s}(x) \,, \tag{A2}$$

where we approximated $g(x) = 1$ for $0 < x < x_0$ to simplify the integration. This simplified expression yields correct behavior for $x \ll 1$. The value of the parameter $x_0 = \sqrt{2}/3$ is set by ensuring energy conservation, i.e., setting $\int_0^1 x\, g(x) dx = \int_0^{x_0} x\, dx$ (we approximate $x_0 \sim 0.5$ in the main text of the paper). Note that the scattered flux distribution for monoenergetic photons computed using this approximation has a maximum at $x = x_0 \approx 0.47$, very close to that of the exact distribution, which peaks at $x \approx 0.61$.

A1. SLOW COOLING

The distribution of seed photons is described by the synchrotron spectrum, which consists of four power-law segments (Sari et al. 1998). Then the inner integral in equation (A2) yields (to a leading order in ν and zeroth order in ν_a/ν_m and ν_m/ν_c)

$$I = \begin{cases} I_1 \simeq \dfrac{5}{2} f_{\max} x_0 \left(\dfrac{\nu_a}{\nu_m}\right)^{1/3} \left(\dfrac{\nu}{4\gamma^2 \nu_a x_0}\right), & \nu < 4\gamma^2 \nu_a x_0 \ ; \\ I_2 \simeq \dfrac{3}{2} f_{\max} x_0 \left(\dfrac{\nu}{4\gamma^2 \nu_m x_0}\right)^{1/3}, & 4\gamma^2 \nu_a x_0 < \nu < 4\gamma^2 \nu_m x_0 \ ; \\ I_3 \simeq \dfrac{2}{(p+1)} f_{\max} x_0 \left(\dfrac{\nu}{4\gamma^2 \nu_m x_0}\right)^{(1-p)/2}, & 4\gamma^2 \nu_m x_0 < \nu < 4\gamma^2 \nu_c x_0 \ ; \\ I_4 \simeq \dfrac{2}{(p+2)} f_{\max} x_0 \left(\dfrac{\nu_c}{\nu_m}\right)^{(1-p)/2} \left(\dfrac{\nu}{4\gamma^2 \nu_c x_0}\right)^{-p/2}, & \nu > 4\gamma^2 \nu_c x_0 \,. \end{cases} \tag{A3}$$

The quantity $f_{\max} = f_{\nu_s}(\nu_m)$ is the flux value at the peak of the synchrotron spectral component. Note that the inverse Compton spectrum for monoenergetic electron scattering has the same frequency dependence above $4\gamma^2 \nu_a x_0$ as the input synchrotron spectrum above the self-absorption frequency, ν_a. In the range $\nu < 4\gamma^2 \nu_a x_0$, the functional form of the differential cross section dominates and I_1 is linear in ν, rather than quadratic.

The integration over different electron energies again needs to be divided into four different regimes:

$$f_\nu^{\rm IC} = R\sigma_T \times \begin{cases} \displaystyle\int_{\gamma_m}^{\infty} d\gamma\, N(\gamma) I_1 \,, & \nu < \nu_a^{\rm IC} \ ; \\ \left[\displaystyle\int_{\gamma_m}^{\gamma_{\rm cr}(\nu_a)} d\gamma\, N(\gamma) I_2 + \int_{\gamma_{\rm cr}(\nu_a)}^{\infty} d\gamma\, N(\gamma) I_1\right], & \nu_a^{\rm IC} < \nu < \nu_m^{\rm IC} \ ; \\ \left[\displaystyle\int_{\gamma_m}^{\gamma_{\rm cr}(\nu_m)} d\gamma\, N(\gamma) I_3 + \int_{\gamma_{\rm cr}(\nu_m)}^{\gamma_{\rm cr}(\nu_a)} d\gamma\, N(\gamma) I_2 + \int_{\gamma_{\rm cr}(\nu_a)}^{\infty} d\gamma\, N(\gamma) I_1\right], & \nu_m^{\rm IC} < \nu < \sqrt{\nu_m^{\rm IC} \nu_c^{\rm IC}} \ ; \\ \left[\displaystyle\int_{\gamma_m}^{\gamma_{\rm cr}(\nu_c)} d\gamma\, N(\gamma) I_4 + \int_{\gamma_{\rm cr}(\nu_c)}^{\gamma_{\rm cr}(\nu_m)} d\gamma\, N(\gamma) I_3 + \int_{\gamma_{\rm cr}(\nu_m)}^{\gamma_{\rm cr}(\nu_a)} d\gamma\, N(\gamma) I_2 + \int_{\gamma_{\rm cr}(\nu_a)}^{\infty} d\gamma\, N(\gamma) I_1\right], & \nu > \sqrt{\nu_m^{\rm IC} \nu_c^{\rm IC}} \,, \end{cases} \tag{A4}$$

where $\gamma_{\rm cr}(\nu) = (\nu/4\nu x_0)^{1/2}$ and the break frequencies are defined as $\nu_a^{\rm IC} = 4\gamma_m^2 \nu_a x_0$, $\nu_m^{\rm IC} = 4\gamma_m^2 \nu_m x_0$, and $\nu_c^{\rm IC} = 4\gamma_c^2 \nu_c x_0$.

Evaluating the integrals in equation (A4) and again keeping only the dominant terms, we obtain

$$f_\nu^{\rm IC} \simeq R\sigma_T n f_{\max} x_0 \times \begin{cases} \dfrac{5}{2}\dfrac{(p-1)}{(p+1)} \left(\dfrac{\nu_a}{\nu_m}\right)^{1/3} \left(\dfrac{\nu}{\nu_a^{\rm IC}}\right), & \nu < \nu_a^{\rm IC} \ ; \\ \dfrac{3}{2}\dfrac{(p-1)}{(p-1/3)} \left(\dfrac{\nu}{\nu_m^{\rm IC}}\right)^{1/3}, & \nu_a^{\rm IC} < \nu < \nu_m^{\rm IC} \ ; \\ \dfrac{(p-1)}{(p+1)} \left(\dfrac{\nu}{\nu_m^{\rm IC}}\right)^{(1-p)/2} \left[\dfrac{4(p+1/3)}{(p+1)(p-1/3)} + \ln\left(\dfrac{\nu}{\nu_m^{\rm IC}}\right)\right], & \nu_m^{\rm IC} < \nu < \sqrt{\nu_m^{\rm IC} \nu_c^{\rm IC}} \ ; \\ \dfrac{(p-1)}{(p+1)} \left(\dfrac{\nu}{\nu_m^{\rm IC}}\right)^{(1-p)/2} \left[2\dfrac{(2p+3)}{(p+2)} - \dfrac{2}{(p+1)(p+2)} + \ln\left(\dfrac{\nu_c^{\rm IC}}{\nu}\right)\right], & \sqrt{\nu_m^{\rm IC} \nu_c^{\rm IC}} < \nu < \nu_c^{\rm IC} \ ; \\ \dfrac{(p-1)}{(p+1)} \left(\dfrac{\nu}{\nu_m^{\rm IC}}\right)^{-p/2} \left(\dfrac{\nu_c}{\nu_m}\right) \left[2\dfrac{(2p+3)}{(p+2)} + \dfrac{2}{(p+2)^2} + \dfrac{(p+1)}{(p+2)} \ln\left(\dfrac{\nu}{\nu_c^{\rm IC}}\right)\right], & \nu > \nu_c^{\rm IC} \,. \end{cases} \tag{A5}$$

There is no abrupt spectral slope change at $\nu = (\nu_m^{\rm IC} \nu_c^{\rm IC})^{1/2}$, so the region with the slope $(1 - p)/2$ extends over twice as many orders of magnitude as the corresponding region in the seed synchrotron spectrum.

It is important to point out that, for $\nu > \nu_m^{\rm IC}$, the presence of logarithmic terms ensures that a broken power law is no longer a good approximation to the correct spectrum.

The value of the flux at the peak of the inverse Compton component is given by

$$f_\nu^{\rm IC}(\nu_m^{\rm IC}) \simeq 4\sigma_T R n f_{\max} x_0 \frac{(p-1)(p+1/3)}{(p-1/3)(p+1)^2}, \tag{A6}$$

assuming that $\nu_a \ll \nu_m \ll \nu_c$.

A2. FAST COOLING

In this regime, the inner integral in equation (A2) evaluates to

$$I = \begin{cases} I_1 \simeq \dfrac{5}{2} f_{\max} x_0 \left(\dfrac{\nu_a}{\nu_c}\right)^{1/3} \left(\dfrac{\nu}{4\gamma^2 \nu_a x_0}\right), & \nu < 4\gamma^2 \nu_a x_0 ; \\ I_2 \simeq \dfrac{3}{2} f_{\max} x_0 \left(\dfrac{\nu}{4\gamma^2 \nu_c x_0}\right)^{1/3}, & 4\gamma^2 \nu_a x_0 < \nu < 4\gamma^2 \nu_c x_0 ; \\ I_3 \simeq \dfrac{2}{3} f_{\max} x_0 \left(\dfrac{\nu}{4\gamma^2 \nu_c x_0}\right)^{-1/2}, & 4\gamma^2 \nu_c x_0 < \nu < 4\gamma^2 \nu_m x_0 ; \\ I_4 \simeq \dfrac{2}{(p+2)} f_{\max} x_0 \left(\dfrac{\nu_c}{\nu_m}\right)^{1/2} \left(\dfrac{\nu}{4\gamma^2 \nu_m x_0}\right)^{-p/2}, & \nu > 4\gamma^2 \nu_m x_0. \end{cases} \tag{A7}$$

Here $f_{\max} = f_{\nu_s}(\nu_c)$.

Performing the appropriate integration over γ we get the spectrum of the inverse Compton emission:

$$f_\nu^{\rm IC} \simeq R\sigma_T n f_{\max} x_0 \times \begin{cases} \dfrac{5}{6}\left(\dfrac{\nu_a}{\nu_c}\right)^{1/3}\left(\dfrac{\nu}{\nu_a^{\rm IC}}\right), & \nu < \nu_a^{\rm IC} ; \\ \dfrac{9}{10}\left(\dfrac{\nu}{\nu_c^{\rm IC}}\right)^{1/3}, & \nu_a^{\rm IC} < \nu < \nu_c^{\rm IC} ; \\ \dfrac{1}{3}\left(\dfrac{\nu}{\nu_c^{\rm IC}}\right)^{-1/2}\left[\dfrac{28}{15} - \ln\left(\dfrac{\nu}{\nu_c^{\rm IC}}\right)\right], & \nu_c^{\rm IC} < \nu < \sqrt{\nu_c^{\rm IC}\nu_m^{\rm IC}} ; \\ \dfrac{1}{3}\left(\dfrac{\nu}{\nu_c^{\rm IC}}\right)^{-1/2}\left[2\dfrac{(p+5)}{(p+2)(p-1)} - \dfrac{2(p-1)}{3(p+2)} + \ln\left(\dfrac{\nu_m^{\rm IC}}{\nu}\right)\right], & \sqrt{\nu_c^{\rm IC}\nu_m^{\rm IC}} < \nu < \nu_m^{\rm IC} ; \\ \dfrac{1}{(p+2)}\left(\dfrac{\nu}{\nu_m^{\rm IC}}\right)^{-p/2}\left(\dfrac{\nu_c}{\nu_m}\right)\left[\dfrac{2}{3}\dfrac{(p+5)}{(p-1)} - \dfrac{2}{3}\dfrac{(p-1)}{(p+2)} + \ln\left(\dfrac{\nu}{\nu_m^{\rm IC}}\right)\right], & \nu > \nu_m^{\rm IC}, \end{cases} \tag{A8}$$

with the break frequencies defined as $\nu_a^{\rm IC} = 4\gamma_c^2 \nu_a x_0$, $\nu_c^{\rm IC} = 4\gamma_c^2 \nu_c x_0$, and $\nu_m^{\rm IC} = 4\gamma_m^2 \nu_m x_0$.

In this regime, the flux at the peak of the inverse Compton component is

$$f_\nu^{\rm IC}(4\gamma_c^2 \nu_c x_0) \simeq \frac{28}{45} \sigma_T R n f_{\max} x_0, \tag{A9}$$

assuming that $\nu_a \ll \nu_c \ll \nu_m$.

APPENDIX B

THE WIND CASE: $\rho \propto R^{-2}$

For the instantaneous spectrum, there is no difference between the ambient medium with a windlike or a constant density profile, since only the density in front of the shock at the time of observation matters. However, the two models clearly have different predictions for the time evolution of the observed emission.

Equation (3.1) and its exact (eq. [3.2]) and approximate (eq. [3.3]) solutions, as well as the expression for η, are valid for any density profile, since they come from the analysis of a "snapshot" spectrum. However, since the time dependence of ν_c/ν_m is different for the windlike and constant density profiles, the evolution of x is different in the two cases and so are the transition times between the three stages. For the wind density profile, the importance of IC emission decreases somewhat faster, since $\nu_c/\nu_m \propto t^2$ in the wind case rather than $\propto t$ as in the constant-density case. This makes the difference between the intermediate regime (slow cooling, IC dominates) and the final regime (slow cooling with negligible IC) more significant.

For the wind profile, the temporal evolution of x is given by

$$x = \sqrt{\frac{\epsilon_e}{\epsilon_B}} \left(\frac{t}{t_0^{\rm IC}}\right)^{-(p-2)/(4-p)}. \tag{B1}$$

Assuming $\epsilon_e \gg \epsilon_B$, slow cooling now lasts until

$$t_0^{\rm IC} = 3.5(1+z)\left(\frac{\epsilon_e}{0.5}\right)^{3/2}\left(\frac{\epsilon_B}{0.01}\right)^{1/2} A_\star \text{ days} , \tag{B2}$$

where we used the Chevalier & Li (2000) notation, $\rho = 5 \times 10^{11}$ g cm^{-3} $A_\star R_{\rm cm}^{-2}$. This is typically longer than in the constant-density case. The IC-dominated stage lasts until

$$t^{\rm IC} = 2.5 \text{ yr}\left(\frac{\epsilon_e/0.5}{\epsilon_B/0.01}\right)^{(4-p)/(p-2)}\left(\frac{\epsilon_e}{0.5}\right)^{3/2}\left(\frac{\epsilon_B}{0.01}\right)^{1/2} A_\star . \tag{B3}$$

This estimate is correct only during the relativistic stage, and the importance of IC cooling declines fast, once the shock speed falls significantly below c.

When inferring the parameters from a snapshot spectrum, the estimate of the total energy and the electron and magnetic energy fractions is not affected by changes in the density profile. Again one has to estimate the combination C as given by equation (4.9) and, provided that $C < \frac{1}{4}$ (otherwise there is no consistent solution), solve for x_1 and x_2 and substitute the values into equation (4.16). The equation for the ambient density also holds, but now it gives the density in front of the shock at the time of observation. However, since this density is not constant in time, the resulting number is not very useful. It is better to compute the normalization coefficient of the $n \propto R^{-2}$ law $A_\star$:

$$A_\star = 3 \times 10^{-3}\left(\frac{\nu_a}{\rm GHz}\right)^{5/3}\left(\frac{\nu_m}{10^{13}\ \rm Hz}\right)^{5/6}\left(\frac{\nu_c}{10^{14}\ \rm Hz}\right)^{1/2} t_{\rm day}^2(1+z)(1+x) , \tag{B4}$$

which is similar to the expression of Chevalier & Li (2000) with an extra factor $(1 + x)$.

For the new IC-dominated solution, given by $x_2 \simeq 1/C \gg 1$, we obtained

$$A_\star = 0.05\eta^{-1}\left(\frac{\nu_a}{\rm GHz}\right)^{-5/3}\left(\frac{\nu_m}{10^{13}\ \rm Hz}\right)^{-4/3}\left(\frac{\nu_c}{10^{14}\ \rm Hz}\right)^{-1}\left(\frac{F_{\nu_m}}{\rm mJy}\right) t_{\rm day}^{-2}(1+z)^{-3} D_{L,28}^2 . \tag{B5}$$

As in the constant-density case, this new solution corresponds to a higher ambient density than the low-x solution.

REFERENCES

Blandford, R. D., & McKee, C. F. 1977, MNRAS, 180, 343
Blumenthal, G. R., & Gould, R. J. 1970, Rev. Mod. Phys., 42, 237
Chevalier, R. A., & Li, Z. Y. 2000, ApJ, 536, 195
Chiang, J., & Dermer, C. D. 1999, ApJ, 512, 699
Dermer, C. D., Bottcher, M., & Chiang, J. 2000a, ApJ, 537, 255
Dermer, C. D., Chiang, J., & Mitman, K. E. 2000b, ApJ, 537, 785
Freedman, D. L., & Waxman, E. 2001, ApJ, in press (astro-ph/9912214)
Galama, T., Wijers, R. A. M. J., Bremer, M., Groot, P. J., Strom, R. G., Kouveliotou, C., and van Paradijs, J. 1998, ApJ, 500, L97
Granot, J., Piran, T., & Sari, R. 1999, ApJ, 527, 236
Katz, J. I. 1994, ApJ, 422, 248
Mészáros, P., & Rees, M. J. 1997, ApJ, 476, 232
Paczyński, B., & Rhoads, J. 1993, ApJ, 418, L5
Panaitescu, A., & Kumar, P. 2000, ApJ, 543, 66
Panaitescu, A., & Mészáros, P. 1998, ApJ, 501, 772
Piran, T. 1999, Phys. Rep., 314, 575
Rybicki, G. B., & Lightman, A. P. 1979, Radiative Processes in Astrophysics (New York: Wiley)
Sari, R., Narayan, R., & Piran, T. 1996, ApJ, 473, 204
Sari, R., Piran, T., & Halpern, J. P. 1999, ApJ, 519, L17
Sari, R., Piran, T., & Narayan, R. 1998, ApJ, 497, L17
Totani, T. 1998, ApJ, 502, L13
Vietri, M. 1997, ApJ, 478, L9
Wei, D. M., & Lu, T. 1998, ApJ, 505, 252
Wijers, R. A. M. J., & Galama, T. J. 1999, ApJ, 523, 177